Numerical modeling of mechanical regain due to self-healing in cement based composites

Giovanni Di Luzio [a, *], Liberato Ferrara [a], Visar Krelani [a, b]

[a] *Department of Civil and Environmental Engineering, Politecnico di Milano, Piazza Leonardo da Vinci 32, 20133 Milan, Italy*
[b] *University for Business and Technology, Kalabria, 10000, Prishtinë, Kosovo*

Recently there has been an increasing interest in self-healing materials which have the ability to retrieve their physico-mechanical properties once the material is damaged. This paper presents a numerical model for the self-healing capacity of cementitious composites capable of simulating the recovery of mechanical properties of the damaged (cracked) material. The recent SMM (Solidification-Micropre-stress-Microplane model M4) model for concrete, which makes use of a modified microplane model M4 and the solidification-microprestress theory, is able to reproduce the concrete time-dependent behavior, e.g. creep, shrinkage, thermal deformation, aging, and cracking from early age up to several years. The moisture and heat fields, as well as the hydration degree, are obtained from the solution of a hygro-thermo-chemical problem which is coupled with the SMM model. This numerical framework is extended to incorporate the self-healing effects and, in particular, the effect of delayed cement hydration, which is the main cause of the self-healing for young concrete. The new update model can also simulate the effects of cracking on the permeability and the opposite restoring effect of the self-healing on the mechanical constitutive law, i.e. the microplane model. A numerical example is presented to validate the proposed computational model employing experimental data from a recent test series undertaken at Politecnico di Milano. The experimental campaign has dealt with a normal strength concrete, in which (by means of three-point-bending tests performed up to controlled crack opening and up to failure, respectively before and after exposure to different conditioning environments) the recovery of stiffness and load bearing capacity has been evaluated.

Keywords:
Concrete cracking
Self-healing
Autogenic healing
Autonomic healing
Hygro-thermo-chemo-mechanical model
Solidification-microprestress-microplane model

1. Introduction

The porous structure of concrete is one of the main causes of its being prone to degradation; even if it is generally accepted that a well-proportioned and properly cured concrete, produced using a low water-to-cement (w/c) ratio, leads to obtain a finished product with good durability performance, no concrete material and structure can be made absolutely waterproof. Because of the porous structure of concrete, water can penetrate through pores and micro-cracks, due to either capillary absorption and/or hydrostatic pressure. Concrete professionals typically adopt the term *permeability* to describe the resistance of concrete to water ingress and/or passage under actual service conditions. This includes the overall permeability issue of concrete including possible existing cracks, due, e.g., to restrained drying shrinkage, thermal deformations as well as sustained service loads.

In view of the aforesaid statements, it would be highly desirable and advantageous to be able not only to *design* and cast a concrete as compact (and impervious) as possible, but also to be capable to provide the material some capacity to reduce its permeability in the cracked state. In this framework, (autogenous or engineering triggered) self-healing cement-based construction materials, able to control and repairing early stage cracks, would represent an exceptional asset to the 21st Century Civil Engineering. Self-sealing/healing of cracks could prevent permeation of driving factors for deterioration and even provide a partial recovery of the engineering properties of the material relevant to the intended applications, thus contributing to extend the service life of the engineering works [1,2].

Discovered as early as in 1836 by the French Academy of Science, and attributed to either delayed hydration of cement/binder, carbonation or the combination of both, many researchers

* Corresponding author.
E-*mail address:* giovanni.diluzio@polimi.it (G. Di Luzio).

Published Journal Article available at: https://doi.org/10.1016/j.cemconcomp.2017.11.006

demonstrated that concrete, under favorable conditions, can heal naturally without any particular additives [1−3]. As a matter of fact, because such a capacity turned out to be quite randomly scattered and thus neither reliable nor predictable in an engineering appli-cation perspective, a paramount effort is currently challenging the concrete research community of investigating "engineering" self-healing capacity of concrete and cement-based construction ma-terials. Several different techniques, along different main directions of investigation, have been conceived and explored: i.e., self-healing engineered with fibre reinforcements [4], mineral-producing bacteria, super absorbent polymers, healing agents contained in shell and tubular capsules and other proprietary chemical admixtures or even mineral additions already tradition-ally employed as cement substitutes [5−9]. The supply of water (moisture) is essential, especially in the case of addition of chemical agents able to promote the deposition of crystals inside the crack, but since most infrastructures are exposed to rain or underground water, usually this is an easily satisfied requirement. Several other variables can affect the phenomenon of self-healing, such as the mix proportions, the stress state along the cracks, the crack open-ing, the thermo-hygrometric conditions, etc. [1,2].

The majority of the research effort on the self-healing phenomenon has been experimentally based up to date but more recently there has been increased interest in developing numerical models to simulate the self-healing processes. In the literature there are very limited numerical studies on this phenomenon. Hilloulin et al. [10] proposed a hydro-chemo-mechanical model based on micro-mechanical observations to evaluate the mechanical properties of the new healing products in order to describe the partial recovery of the mechanical properties of healed ultra high performance concrete (UHPC). However, in this model the effect of the crack opening and the temperature are not considered and the model is limited only to autogenous healing. The same authors in Ref. [11] presented a finite element model to characterize the micro-mechanical properties of the healing products based on the coupling of the microstructural hydration model CEMHYD3D and the finite element code Cast3M. On the whole the numerical simulation were in agreement with the experimental observation on the healing potential and rate, and on the nature of the healing products. In Ref. [12] to model the self-healing behavior, an uncoupled physico-chemical based healing model for concrete is developed and implemented. The model is based on the fact that the healing mechanism is activated through precipitation of calcium carbonate inside the cracks. However, the authors presented only preliminary results which show a qualitatively good agreement with some experimental evidences. A micro-mechanical constitutive model incorporating the self-healing by using a solidification formulation was recently proposed in Ref. [13]. The model was successfully applied to simulate the recovery of mechanical properties of the micro-cracked material. However, this model does not take into account diffusion processes and is limited to autogenous healing. Recently a damage-plasticity constitutive theory for zero-thickness interfaces has been proposed [14] in which the self healing effects are modeled through a calibrated time evolution of the concrete open porosity.

The SMM (solidification-Microprestress-Microplane model M4) model [15] for concrete, which makes use of the microplane model M4 and the solidification-microprestress theory, is able to reproduce, as shown, all the relevant aspects of the time-dependent concrete behavior, such as creep, shrinkage, thermal deformation, aging, and cracking starting from the very early ages and up to several years. The moisture and heat fields, as well as the cement hydration degree are obtained from the solution of the hygro-thermo-chemical problem [16,17].

This computational framework has been extended in this paper in order to incorporate the self-healing effects introducing an internal variable which characterizes the self-healing process, the effects of cracking on the diffusivity, and the positive recovering effect of the self-healing on the mechanical properties. The model in the initial and updated stages of its development was presented at some recent conferences [18−20]. A numerical example is herein presented to validate the proposed model and to show its capability of correctly capturing the outcomes of self-healing in terms of re-covery of the mechanical properties. Reference has been made to a recent experimental investigation carried out in our laboratory [21] in which normal strength concrete, both without and with a crys-talline admixture used as a self healing promoter, has been utilized. Concrete was cured under constant relative humidity, first stored in a room at 90% RH up to about 28 days and then, after pre-cracking, immersed in water or exposed to open air. A methodology has been developed to assess the capacity of the material to recover its pristine levels of mechanical performance. With reference to three-point bending tests performed up to controlled crack opening and up to failure (respectively before and after exposure to the different conditioning environments) the recovery of stiffness and load bearing capacity have been evaluated to assess the self-healing capacity [21]. Using these experimental results, the proposed model is calibrated and validated in order to have a numerical tool that can be utilized to assess structural applications which incorporate the self-healing concept to enhance the durability and service life of reinforced and pre-stressed concrete structures.

2. Multi-physics formulation of SMM model and self-healing model

The SMM formulation [15] is made up of a multi-physics model that is capable of reproducing the time dependent behavior of concrete, including creep and relaxation, cracking and damage, hygral and thermal deformations, heat production and diffusion, moisture variation and diffusion, and aging.

2.1. Heat transfer and moisture diffusion

The behavior of concrete, starting from very early age, relies very much on the internal relative humidity, h, and the temperature, T, whose evolutions and distributions can be evaluated, in the considered domain, by enforcing the moisture content mass balance and enthalpy balance, respectively. Considering a concrete mixture with a binder which is only Portland cement and with a temperature which not exceeds 90°C, the two mass balance equations can be expressed as [16]

$$\nabla\cdot(D_h\nabla h) - \frac{\partial w_e}{\partial h}\frac{\partial h}{\partial t} - \frac{\partial w_e}{\partial \alpha_c}\dot{\alpha}_c - \dot{w}_n = 0 \tag{1}$$

and

$$\nabla\cdot(\lambda_t\nabla T) - \rho c_t\frac{\partial T}{\partial t} + \dot{\alpha}_c\ c\ \tilde{Q}_c^{\infty} = 0 \tag{2}$$

where D_h is moisture permeability, w_e is evaporable water content (see Appendix A), $\alpha_c =$ is the hydration degree, $\dot{w}_n = 0.253\dot{\alpha}_c c$ is the rate of non-evaporable water, ρ is the mass density of concrete, c_t is the isobaric heat capacity (specific heat), λ_t is the heat conductivity, c is the cement content, and $\tilde{Q}_c^{\infty}$ is the latent heat of cement reaction per unit mass of reacted cement. All the details of this formulation can be found in Ref. [16] and, in addition, more information about its calibration and validation are reported in Ref. [17].

2.2. Cement hydration

In the concrete mixture considered in this study, the main chemical reaction is the cement hydration which is the reaction between the free water and the unhydrated cement particles. The main products of this reaction are the calcium hydroxide (C-H) and the Calcium-Silicate-Hydrates (C-S-H). The latter is the principal component of the solid cement paste which provides the stiffness and the strength of concrete.

The hydration degree, α_c, which represents the fraction of reacted cement, describes the overall cement hydration process [16,22–24]. The evolution equation for the hydration degree can be expressed as

$$\dot{\alpha}_c = \frac{A_{c1} e^{-\eta_c \alpha_c / \alpha_c^\infty} e^{-E_{ac}/RT}}{1 + (5.5 - 5.5h)^4} \left(\frac{A_{c2}}{\alpha_c^\infty} + \alpha_c \right) (\alpha_c^\infty - \alpha_c) \tag{3}$$

where E_{ac} is the hydration activation energy, R is the universal gas constant, η_c, A_{c1}, A_{c2} are material parameters, and α_c^∞ is the asymptotic value of the hydration reaction degree. The asymptotic degree of cement hydration, α_c^∞ (the value of hydration degree reached at infinite time), can be evaluated as $\alpha_c^\infty = (1.032w/c)/(0.194 + w/c)$ where w/c is water to cement ratio [16,25].

2.3. Self-healing

In this Section after a description of the self-healing processes in cementitious materials the extension of the formulation in order to simulate those phenomena is presented.

2.3.1. Self-healing phenomena in cement-based materials

The model formulation proposed in this paper considers both autogenic healing (phenomenon in which cracks in concrete are naturally clogged in an environment involving moisture without any special arrangement in the material design) and autonomic/engineered healing (phenomenon in which cracks are clogged in concrete made with special material additives to accelerate the clogging of cracks in the concrete in an environment rich in moisture). The self-closing of a crack can occur because of physical, chemical and mechanical causes. The physical cause is due to swelling of hydrated cement paste near the crack surface. On the chemical side, two main phenomena are responsible for crack sealing/healing. The first one is the hydration of cement grains which has not still reacted. When they react the new products occupy the half room of the original cement grains progressively filling the free space in the crack. This process can give, together with the swelling of hydrated cement paste, a complete closing of the crack only if the crack width is less than 0.1 mm [1]. The second chemical process is the formation of calcium carbonate and the growth of crystals on the crack surface. This reaction, that depends on the temperature, pH, and concentration of the reactants, is considered by many authors [1,26] the most important mechanism in the self-healing process. Finally there are also two minor mechanical processes that contribute to the self-healing: the presence of fine particles in the water which may leak through the crack and the fracturing of small concrete particles from the crack faces [1]. The previous description of the mechanisms that contribute to the self-healing highlights the determinant contribution of water, which is needed for the chemical reactions, for the transport of fine particles and for the swelling of hydrated cement paste.

For the sake of synthesis it can be said that the healing phenomenon is a water driven process and that its kinetics is governed by the chemical reactions, such as hydration of un-hydrated cement grains and the production of calcium carbonate as described above, which can be promoted by supplying additional materials in the mixture, as done in the experimental campaign herein considered as reference (see Section 3).

The overall self-healing process is here described by the normalized reaction extent λ_{sh} which is termed the self-healing recovery degree. This variable characterizes the evolution of the healing repairing process with $\lambda_{sh} = 0$ at the beginning and $\lambda_{sh} = 1$ at the full completion of the process. The self-healing recovery degree describes the healing repairing with reference to the regaining in terms of the strength after its reduction due to damage/cracking (strength restoration). This means that if $\lambda_{sh} = 1$ at the end of the healing process the material recovers completely from damage/cracking deterioration as a virgin material. When cracks are repaired due to autogenic healing or autonomic healing, the mechanical properties after healing will be in most cases inferior compared to virgin specimens. Moreover, though the materials which fill the crack (secondary hydration products and $CaCO_3$ crystals) are identical to the constituting elements of the cementitious matrix, CSH gel formed due to ongoing hydration seems to have lower mechanical properties compared to primary hydration products, and deposited $CaCO_3$ crystals do not form a proper bond with the crack faces. This implies that for autogenic healing mechanical properties of the virgin material will never be regained completely, i.e. $\lambda_{sh} < 1$ at the end of the process. Only in case of autonomic or engineered healing the complete regain in strength and stiffness can be obtained or even a performance higher than that of the virgin material [27–29].The regain of the direct tensile strength of cement paste specimens has been measured in Ref. [30] at different ages, from 1 to 90 days. Specimens fractured at 1 day were healed in water or 95% RH and then fractured in direct tension once again after 7 days, 28 days and 90 days. Specimens fractured at 7 days were healed and re-fractured at 28 and 90 days. Specimens fractured at 28 days were healed and re-fractured at 90 days. During healing the two pieces of each fractured specimen were held together by a rubber band. The results showed that the maximum healing, about 25%, was obtained for specimens fractured at 1 day and re-tested at 90 days. Healing performed at 95% RH gave much smaller regain with a maximum healing only about 4%.

2.3.2. Self-healing model

The driving force of the overall healing process is the reaction affinity $A_{sh}(\lambda_{sh})$ that can reasonably be assumed to decrease progressively from an initial value $A_{sh}(\lambda_{sh} = 0) = A_{sh0}$ that starts the reaction up to an equilibrium state $A_{sh}(\lambda_{sh} = 1) = 0$ when the healing process ceases. Assuming the affinity to vary linearly it reads

$$A_{sh}(\lambda_{sh}) = A_{sh0}(1 - \lambda_{sh}) \tag{4}$$

Additionally, a linear relationship is also adopted between the reaction rate $\dot{\lambda}_{sh}$ and the reaction affinity

$$A_{sh}(\lambda_{sh}) = k_{sh}\dot{\lambda}_{sh} \tag{5}$$

where k_{sh} is a positive kinetic coefficient. Substituting $A_{sh}(\lambda_{sh})$ in Eq. (4) yields a reaction kinetic law of first order [31]

$$\dot{\lambda}_{sh} = \tilde{A}_{sh}(1 - \lambda_{sh}) \tag{6}$$

where $\tilde{A}_{sh} = A_{sh0}/k_{sh}$ represents the inverse of the characteristic time of the overall self-healing reaction. To set up a reasonable and physically sound expression for the initial reaction affinity A_{sh0} and, consequently, for the coefficient $\tilde{A}_{sh}$, it has to be considered that, as

it is explained above, this coefficient depends on many different factors. (1) The extent of self-healing in cracked concrete was found to be highly dependent on the crack width, with smaller cracks healing generally better and at a faster rate than larger cracks. In some cases with small crack widths, cracks may autogenously heal completely, thus increasing the durability and potentially the mechanical properties of the damaged material [32–35]. (2) Based on the results of the experimental data in [30] and [36] the continued hydration is the principal cause of recovery. (3) The other fundamental process generating the self-healing is the calcium carbonate precipitation which is a rather straightforward chemical process governed mainly by four key factors: the calcium concentration, the concentration of dissolved inorganic carbon, the pH, and the availability of nucleation sites [1,26]. (4) [37] and [30] showed from their experimental investigation that the moisture supply is the most important factor for self-healing and that the age of the first cracking is also of the utmost importance. Therefore, from those evidences in the literature, the quantities of unhydrated cement at the time of first crack and the moisture content in the pores of concrete near the crack are the essential parameters for the autogenic healing process.

Extensive experimental work on healing of cracks with regard to permeability has been performed by Ref. [32]. Considering the flow through specimens with one single crack parallel to water flow at the water pressure equal to 0.025 MPa, complete healing was observed after about 200 h for the crack width 0.10 mm. Also cracks with 0.20 and 0.30 mm width healed almost completely within about 30 days. The influence of temperature and crack width on self-healing has been investigated by Ref. [33] showing that the decrease of the flow rate depends on crack width and temperature, i.e. smaller cracks do heal faster than greater ones and a higher temperature favors a faster self-healing process. The type of cement, the type of aggregates, and the mechanical pressure gradient have hardly any effect on the autogenic self-healing [32].

In the case of autonomic healing the cracks are clogged in concrete made with special material design, such as the use of an appropriate supplementary cementing material in expectation of its effect of clogging or accelerating the clogging of cracks in the concrete.

According to the evidences recalled above the coefficient $\tilde{A}_{sh}$ can be expressed as

$$\tilde{A}_{sh} = \tilde{A}_{sh0}\, f_h(h)\, f_w(w_c)\, e^{\frac{-E_{sh}}{RT}} \tag{7}$$

The fourth term in Eq. (7), expressing effect of current temperature, T, on the reaction rate, is of the Arrhenius type, as usual for thermally activated chemical reactions where E_{sh} is the self-healing activation energy and R is the universal gas constant. The coefficient $\tilde{A}_{sh0}$ accounts the effect of the initial unhydrated cement and the possible presence of additive material that accelerates the healing process

$$\tilde{A}_{sh0} = \tilde{A}_{sh1}\left(1 - \alpha_c^{sh0}\right)c + \tilde{A}_{sh2}\; ad \tag{8}$$

where α_c^{sh0} is the value of the hydration degree when the healing process starts (that isn't generally uniform in the volume), c is the cement content, so the product $(1-\alpha_c^{sh0})c$ represents the amount unhydrated cement when the healing action begins, ad is the content of healing boosting additive, and $\tilde{A}_{sh1}$ and $\tilde{A}_{sh2}$ are two material parameters that have the units of volume/mass/time. The first term in Eq. (8) weights the effect of all the chemical processes as described above. Here the effect of any supplementary "healing engineering" admixture is considered to be additive to the effect of the unhydrated cement because of the type of additive used in the experimental campaign (see section 3). Different kind of additives may give different contribution to the affinity. It is well known from experiments the importance of water or high level of relative humidity to activate the self-healing activity which, below a certain value, decreases and may be even zero. This is taken into account in this model by means of the coefficient $f_h(h)$, also used in the definition of the hydration degree, and which is given by

$$f_h(h) = \frac{1}{1 + (a_h - a_h h)^{b_h}} \tag{9}$$

where the parameters a_h and b_h are assumed constant and equal to 8 and 4, respectively, from a best fitting of the experimental data. The function $f_h(h)$ is plotted in Fig. 1a. This formula expresses that when the relative humidity is only 95% the extent of healing is already much lower as reported by Ref. [30]. The effect of the initial value of the crack width is reproduced by the coefficient $f_w(w_c)$ which has the following expression

$$f_w(w_c) = \left\{1 + [a_w - a_w(1 - w_c)]^{b_w}\right\}^{-1} \tag{10}$$

with the addition that the self-healing activity $f_w(w_c) = 0$ as far as $w_c < w_{c0}$. The coefficients a_w and b_w are two free parameter. The expression of the function in Eq. (10) (plotted in Fig. 1b) has been formulated on the basis of experimental data on the maximum crack width that can be healed by autogenic healing which was observed to differ substantially among reports made by various authors, i.e., from 5 to 10 μm [38,39], 100 μm [33], 200 μm [32], and 300 μm [40]. Moreover, as also shown by Ref. [41], the presence of a through crack stress may favor (if compressive) or not (if tensile) the effect of healing [42]. In this formulation only stress-free cracks have been considered.

Other influencing factors of the healing processes, which are not taken into account in the actual formulation of the proposed model, are: (1) the water pressure, a fast liquid flowing through the crack would prevent the self healing from occurring, because the liquid would wash out the deposited healing products [43,44]; (2) the leaching or dissolution, a liquid that leads to a leaching or dissolution reaction can affect the healed crack and this phenomenon is neglected; (3) the stability of the crack over time, since the crack opening has to be more or less constant in order to have the healing it is assumed that the cracks keep their initial opening.

2.4. Mechanical behavior

If the hypothesis of strain additivity holds [15] the total strain rate, $\dot{\varepsilon}$, can be written in the following format

$$\dot{\varepsilon} = \dot{\varepsilon}^i + \dot{\varepsilon}^v + \dot{\varepsilon}^f + \dot{\varepsilon}^d + \dot{\varepsilon}^s + \dot{\varepsilon}^t \tag{11}$$

where $\dot{\varepsilon}^i$ is the instantaneous strain rate, $\dot{\varepsilon}^v$ is the viscoelastic strain rate, $\dot{\varepsilon}^f$ is the purely viscous strain rate, $\dot{\varepsilon}^d$ is the inelastic strain rate due to smeared crack or damage, $\dot{\varepsilon}^s$ and $\dot{\varepsilon}^t$ are hygral and thermal strain rates caused by the variations of relative humidity and temperature, respectively. The strain additivity assumption, in Eq. (11), is equivalent to a rheological model in which all the elements are coupled in series with a constant stress in the elements of the chain.

In the proposed model, it is assumed that the material healing is only affecting the microplane model and does not have any effect on the creep model. This is consistent with the basic assumption of the SMM model in which the series coupling reproduces in a smeared way what happens in the crack band: damaging (fracturing) in the localized crack plus linear creep (visco-elasticity) of

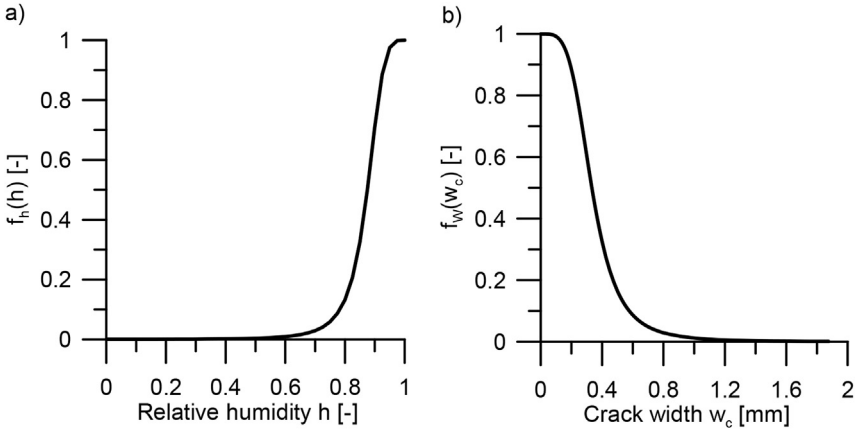

Fig. 1. Effect of (a) relative humidity and (b) crack opening on the healing process affinity.

the material undamaged bulk.

2.4.1. Microprestress-solidification theory

The instantaneous strain rate, $\dot{\varepsilon}^i$, is the strain rate which shows up directly after the application of a stress rate, $\dot{\boldsymbol{\sigma}}$, and it can be formulated as age independent with the following expression: $\dot{\varepsilon}^i = q_1 \mathbf{G}\dot{\boldsymbol{\sigma}}$, in which the material parameter q_1 (in MPa^{-1}) represents the inverse of the instantaneous stiffness and can be considered age independent at typical room temperatures and for saturation condition (see Ref. [45]). Because the material isotropy is also preserved for visco-elastic deformation, the matrix $\mathbf{G}$ is the elastic compliance matrix with a unit Young modulus and constant Poisson's ratio (the value of $\nu = 0.18$ is hereinafter utilized):

$$\mathbf{G} = \begin{bmatrix} 1 & -\nu & -\nu & 0 & 0 & 0 \\ -\nu & 1 & -\nu & 0 & 0 & 0 \\ -\nu & -\nu & 1 & 0 & 0 & 0 \\ 0 & 0 & 0 & 2(1+\nu) & 0 & 0 \\ 0 & 0 & 0 & 0 & 2(1+\nu) & 0 \\ 0 & 0 & 0 & 0 & 0 & 2(1+\nu) \end{bmatrix} \tag{12}$$

The dominating aging creep at early age is due to the gel deformations during its formation, which can be described by the solidification theory [46] through the viscoelastic strain rate, $\dot{\varepsilon}^v$, and it can be expressed as

$$\dot{\varepsilon}^v(t) = \frac{1}{v(\alpha_c)}\ \dot{\boldsymbol{\gamma}} \quad \text{and} \quad \boldsymbol{\gamma} = \int_0^t \Phi(t-\tau)\mathbf{G}\dot{\boldsymbol{\sigma}}\mathrm{d}\tau \tag{13}$$

where $\dot{\boldsymbol{\gamma}}$ is the viscoelastic micro-strain rate of cement gel assumed to be age-independent and $v(\alpha_c)$ is the aging function, which characterized the aging effect due to the growth of hydration products and represents the volume fraction of cement gel produced by early-age chemical reactions and, as a consequence, it can be assumed as a function of the hydration reaction degree, α_c.

According to [46], the non-aging micro-compliance function of hydrated cement gel can be formulated as $\Phi(t-t_0) = q_2 \ln[1+(t-t_0)^{0.1}]$, in which q_2 (in MPa^{-1}) is a material parameter and $t-t_0$ is the loading time duration. It should be remarked that the viscoelastic strain of the cement gel, $\boldsymbol{\gamma}(t)$ in Eq. (13), is fully recoverable upon unloading, on the contrary, the macroscopic viscoelastic strain, ε^v, is only partially recoverable because of the aging effect reproduced by the aging function $v(\alpha_c)$. Based on the solidification theory [46] the aging effect on stiffness and creep is modeled directly by the simulation of the volume growth of solidified material at early age using the aging function introduced in Eq. (13). A suitable expression of this aging law is

$$\frac{1}{v(\alpha_c)} = \left[\frac{\alpha_c^{\infty}}{\alpha_c}\right]^{n_\alpha} \tag{14}$$

where n_α is a material parameter that can be calibrated by simulating experimental data on aging basic creep [15].

In addition to the aging viscosity due to volume growth of hydration products, there is also the aging viscosity resulting from the relaxation of micro-prestress, which is modelled through the purely viscous strain rate, $\dot{\varepsilon}^f$. This strain represents the completely irrecoverable part of the creep deformation and it has been explained by the effect of the micro-prestress on the slippage between adsorbed water layers hindered in cement nanopores. The concept of micro-prestress, S, was introduced by Bažant and coworkers [47,48] and it represents an average measure of the stress acting transversally on the nanopore bonds that, with its variations, can promote or prevent the slippage between adsorbed water layers. Therefore under general temperature and relative humidity variations the purely viscous creep strain rate and the evolution of micro-prestress can be expressed by the following formulae [48].

$$\dot{\varepsilon}^f = q_4\kappa_0 S\mathbf{G}\boldsymbol{\sigma} \text{ and } \dot{S} + \kappa_0 S^2 = \kappa_1 \left|\dot{T}\ \ln h + T\ \dot{h}/h\right| \tag{15}$$

where the material parameters κ_0 (in MPa^{-1} day^{-1}), κ_1 (in MPa K^{-1}), and q_4 (in MPa^{-1}) need to be calibrated from relevant experimental data. Note that while the general formulation depends separately on κ_0, κ_1, and q_4, only parameter q_4 governs long-term basic creep behavior [48]. It is worth noting that only the parameter q_4 governs long-term basic creep behavior [48] while the general formulation depends on the parameters κ_0, κ_1, and q_4, separately.

2.4.2. Microplane model for damage (and cracking)

Damage and smeared crack strain, ε^d, is obtained through a modified version of the Microplane Model M4 [49,50]. With regard to the coupling between the microplane theory with the previous formulation, Eq. (11) can be conveniently rewritten as:

$$\dot{\varepsilon} = \dot{\varepsilon}^i + \dot{\varepsilon}^v + \dot{\varepsilon}^f + \dot{\varepsilon}^m - \dot{\varepsilon}^e + \dot{\varepsilon}^s + \dot{\varepsilon}^t \tag{16}$$

where $\dot{\varepsilon}^e = \overline{E}^{-1}\mathbf{G}\dot{\boldsymbol{\sigma}}$ is an average elastic strain rate that needs to be subtracted from the strain rate obtained from the microplane model in order to take only the cracking/damage strain: $\dot{\varepsilon}^d = \dot{\varepsilon}^m - \dot{\varepsilon}^e$. Based on the original microplane formulation, the

modulus $\bar{E}$ has the meaning of an average elastic modulus and is utilized as dimensional parameter in the microplane limit curves [49]. In the present formulation $\bar{E}$ does not have physical meaning, because it is introduced only for numerical convenience, and it can be estimated as the concrete Young modulus at 28 days before the model calibration without any loss of generality.

In a kinematically constrained microplane model the strain vector on each microplane is obtained from the projection of the macroscopic strain tensor on that plane. Using a matrix notation the following macro-micro relation holds [51]:

$$\boldsymbol{\varepsilon}_{\mathscr{P}} = \mathscr{P}\varepsilon^m \tag{17}$$

where $\boldsymbol{\varepsilon}_{\mathscr{P}} = [\varepsilon_N\ \varepsilon_M\ \varepsilon_L]^T$ is the microplane strain vector on the generic plane having an orientation characterized by its unit normal n_i, with ε_N as normal strain component, ε_M and ε_L as shear strain components, and the matrix $\mathscr{P}$ contains the components of the tensors $N_{ij} = n_i n_j$, $M_{ij} = (m_i n_j + m_j n_i)/2$ and $L_{ij} = (l_i n_j + l_j n_i)/2$, in which n_i, m_i, and l_i are unit vectors defining a local cartesian coordinate system on a generic microplane.

Formulating appropriate constitutive equations at microplane level the microplane stress vector, $\boldsymbol{\sigma}_{\mathscr{P}} = [\sigma_N\ \sigma_M\ \sigma_L]^T$, can be evaluated for each microplane, then the macroscopic stress tensor can be calculated using the principle of virtual work:

$$\boldsymbol{\sigma} = \sigma_V \mathbf{I} + \frac{3}{2\pi}\int_{\Omega} \mathscr{D}^T(\boldsymbol{\sigma}_{\mathscr{P}} - \sigma_V \mathbf{I}_{\mathscr{P}})\,\mathrm{d}\Omega \tag{18}$$

where Ω is the surface of a unit hemisphere, $\sigma_V = \sigma_{ii}/3$ is the volumetric stress, $\mathbf{I} = [1\ \ 1\ 1\ 0\ 0\ 0]^T$, $\mathbf{I}_{\mathscr{P}} = [1\ 0\ 0]^T$, $\mathscr{D} = \mathscr{P} - \mathscr{V}$, $\mathscr{V}_{11} = \mathscr{V}_{22} = \mathscr{V}_{33} = 1/3$ and $\mathscr{V}_{ij} = 0$ otherwise. Additional details of the adopted microplane constitutive equations can be found in Appendix B and in following references: [49,50,52,53].

The macroscopic stress tensor can be expressed formally as $\boldsymbol{\sigma} = \mathbf{F}(\varepsilon^m)$ where the function $\mathbf{F}()$ represents the microplane model formulation. As a consequence the microplane strain rate can be written as

$$\dot{\varepsilon}^m = \left(\frac{\partial \mathbf{F}}{\partial \varepsilon^m}\right)^{-1} \dot{\boldsymbol{\sigma}} \tag{19}$$

Generally the gradient of the function $\mathbf{F}$ cannot be derived analytically and, therefore, $\dot{\varepsilon}^m$ must be calculated numerically [52].

A constitutive law that must be able to reproduce the concrete behavior starting from the early age has to take into account the aging phenomenon that represents the changes in the macroscopic behavior directly related to the evolution of nano- and micro-scale physical mechanisms and chemical reactions. Macroscopically the aging is manifested as (1) a stiffness increases with creep decreases with age; (2) concrete strength, in tension and compression, and fracture energy increase with age; (3) volume, size, and interconnectivity of pores at different scales change, as a consequence, there is a change in the material properties relevant to moisture diffusion and heat transfer. In this model, the effect of aging on both mechanical and hygro-thermal behavior is modeled in a unified manner through the hydration degree. The effect of aging on stiffness and creep is modeled through the solidification theory as previously presented. The evolution of strength and fracture energy at early age is simulated using the aging degree, λ,defined as [16,23].

$$\dot{\lambda} = \begin{cases} \left(\dfrac{T_{max} - T}{T_{max} - T_{ref}}\right)^{n_\lambda} (B_\lambda - 2A_\lambda \alpha_c)\dot{\alpha}_c & \text{if} \quad \alpha_c > \alpha_0, \\ 0 & \text{if} \quad \alpha_c \le \alpha_0. \end{cases} \tag{20}$$

The parameter α_0 defines the value of the hydration degree at the beginning of the solidification phase. Typically in the literature the values of $\alpha_0 = \frac{0.1}{0.4}$ have been utilized based on the different type of cement and water/cement ratio [54]. T_{max} is the maximum temperature at which hardening of concrete is possible under standard conditions ($\approx 95^\circ$C). T_{ref} is the reference temperature for the experimental calibration of the aging model, thus for $T = T_{ref}$, we must have $\lambda = 0$ for $\alpha_c \le \alpha_0$ and $\lambda = 1$ for $\alpha_c = \alpha_\infty$. From these initial and final conditions one obtains $B_\lambda = [1 + A_\lambda(\alpha_c^{\infty^2} - \alpha_0^2)]/(\alpha_c^\infty - \alpha_0)$, in which only α_0, n_λ, A_λ are model parameters which are needed to be calibrated from relevant experimental data.

The concept of aging degree is here utilized in order to consider the early age phenomena within the modified microplane model M4 formulation. This is obtained by making some material parameters of the model, k_1 through k_7, which govern the microplane constitutive relations (stress-strain boundaries), function of the aging degree, λ, see Appendix B for a brief description and [15] for further details.

2.4.3. Self-healing damage recovery

The microplane model M4 [49] formulation is based on some constitutive relations which are defined on each microplane through incremental elastic relations between stress and strain and through limit curves, called stress-strain boundaries (softening/hardening yield limits), that cannot be exceeded. For all intents and purposes, the stress-strain boundaries can be considered as strain dependent yield limits [55]. In order to account for the effect of the healing processes on the mechanical properties of concrete, the aforementioned stress-strain boundaries are updated. In particular the boundary, F_N, on the normal components, σ_N and ε_N, which is imposed the condition $\sigma_N \le F_N(\varepsilon_N)$, and the cohesion in the friction boundary, $\sigma^0{}_N$, are modified (see Appendix B for the details on those boundaries). To introduce the recovery of the strength produced by the healing phenomena the formulation of those boundaries are not modified instead their current values are calculated as $F_N(\varepsilon_N - \varepsilon_N^{sh})$ and $\sigma_N^0(\varepsilon_I - \varepsilon_I^{sh})$. In those expressions ε_N^{sh} is calculated as $\varepsilon_N^{sh} = \lambda_{sh}\varepsilon_N^*$ and ε_I^{sh} is the maximum principal strain of the tensor ε^* multiplied by λ_{sh} in which ε^* is the value of strain tensor reached at the end of the cracking stage and λ_{sh} is the value of the self-healing recovery degree during the healing activity. In Fig. 2 the evolution of healing effect on the normal component is shown, in which the black continuous curve represents the stress-strain boundary and the red dashed curve is the evolution of the normal stress in the cracking stage (Fig. 2a). The purple continuous curve in Fig. 2b represents how the healing effect modified the evolution of the normal component when the normal strain increases.

The SMM model is particularly suitable for time dependent behavior of concrete such as creep and relaxation, especially in the non-linear situation, i.e. tertiary creep, and under variation of temperature and relative humidity. As demonstrated in Ref. [52], the nonlinearity of concrete creep associated with a high stress level is only apparent, since it is caused by a combination of two phenomena: (1) the rate-dependent fracturing of microcrack growth explained by the activation energy of bond ruptures (rate-dependent microplane model); and (2) the linear creep of the bulk of the material (for constant temperature and relative humidity). Under sustained mechanical action, the proposed modifications for self-healing phenomena introduce a change in the evolution of the microcrack growth in which a regain of strength withstand the crack propagation. As consequence, a competition between crack propagation and healing processes with crack closure (and strength recovery) leads to a modification of the tertiary creep evolution which now depends on the rates of the two competing phenomena. Surely, the effect of self-healing on the evolution of crack growth

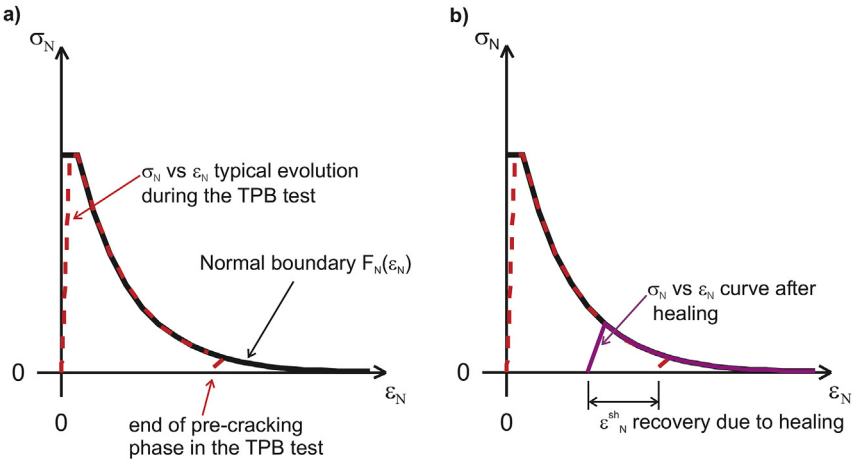

Fig. 2. Effect of self-healing on constitutive law of microplane normal components: before, (a), and after, (b), the healing process.

under sustained loads would be subject of future work, especially because this condition represents a concrete in a real structure under service loading.

2.4.4. Hygral and thermal deformations

Variation of moisture content in the cement paste pores causes changes in capillary tension, surface tension, and disjoining pressure, and, as a consequence, free hygrometric strain ε^s (swelling or shrinkage, for positive or negative relative humidity change, respectively) is macroscopically observed. The hygrometric strain can be written as $\dot{\varepsilon}^s = k_{sh}\dot{h}\mathbf{I}$ where the coefficient k_{sh} can be assumed as constant because, in the literature, there is a lack of an established formulation for such a dependence. In addition, temperature changes cause thermal strain rates as well. Thermal strain rates can be formulated as $\dot{\varepsilon}^t = k_t\dot{T}\mathbf{I}$ where the coefficient k_t is assumed to be also constant. This approximation holds for moderate temperature variations although some deviation has been observed as function of temperature, relative humidity, and aging [56].

2.5. Hygro-thermo-mechanical coupling

The solution of the hygral-thermal-chemo model provides all the physical fields that are utilized in the mechanical model as previously described, i.e. temperature, relative humidity, hydration degree, and self healing reaction degree. Since the temperature range considered in this formulation is relatively low (below $90^\circ C$ and above $0^\circ C$), the direct influence of temperature on the macroscopic mechanical properties of concrete can be neglected. However, the dependence of the microplane model on the aging degree accounts for the aging under different curing conditions (see Appendix B for a brief description and [15] for further details). Similarly, the influence of relative humidity condition is also accounted for in the model.

The water diffusion, which is described by Eq. (1), is as a matter of fact influenced heavily by damage/crack. So far, even if this effect has been neglected in the original hygro-thermo-chemical model [16], it showed a good capability to fit the experimental data. As demonstrated in Ref. [17] the hygro-thermo-chemical model is able to simulate the moisture drying from early ages observed in Refs. [57,58,59], and the moisture loss of different cylindrical concrete specimens of [60]. However, in view of the modeling of the healing activity in cement based materials, the dependence of permeability on the damage and crack opening have to be explicitly taken into account because of the high localized character of the healing processes. Since a continuous approach is utilized for the hygro-thermo-chemo-mechanical modeling the influence of damage/crack need to be smeared-out and treated as an average solution of the problem in the localization zone. In the proposed model it is assumed that only the moisture permeability coefficient is affected by the crack width (damage) of concrete, which is calculated from the mechanical model, i.e. modified aging microplane model M4 for concrete [15,50]. At present, there are some experimental data that are relevant to measurements of the permeability in cracked and fully saturated concrete [34,43,44,61,62]. The effect of cracking on the overall moisture permeability is described by multiplying D_h (moisture permeability of uncracked concrete) by a normalized permeability coefficient, $f_D(w_c)$, which depends on the crack width w_c. On the basis of those experimental results, the expression of the normalized permeability coefficient can be obtained by dividing the permeability coefficient corresponding to cracked concrete by that of the uncracked concrete. A fair expression of $f_D(w_c)$ that gives a satisfactory fitting of the experimental data is given by

$$f_D(w_c) = 1 + \frac{999e^{n_c\xi}}{1-(1-e^{n_c})\xi} \text{ with } \xi = \min\left[\frac{\max(w_c - w_{c0}; 0)}{w_{c1} - w_{c0}}; 1\right] \tag{21}$$

where the parameter n_c governs the shape and slope of the

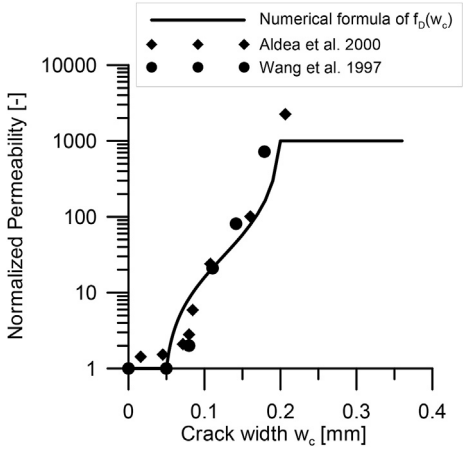

Fig. 3. Normalized permeability as function of the crack opening.

coefficient $f_D(w_c)$, which is plotted in Fig. 3 for $n_c = -3.5$ that gives the best fitting of the experimental data [34,61]. The expression in Eq. (21) gives a constant permeability (of uncracked concrete), i.e. $f_D(w_c) = 1$, as far as the crack width is smaller than $w_{c0} \approx 0.05$ mm. As soon the crack width w_c exceeds the threshold value w_{c0} the water permeability of concrete rapidly jumps up to its maximal value, which is assumed to be about 1000 times the value for uncracked concrete. This value is reached for a critical crack width, $w_{c1} \approx 0.2$ mm. It is assumed that a further increase of the crack width doesn't cause an increase of the permeability which remains thereafter constant, i.e. the crack width is so wide that no significant additional increase of the moisture flow can be obtained from an increase of the crack opening.

Because the moisture transport is described by a Fick's first law for continuous porous materials and that model is extended to include the effect of smeared (not discrete) cracks, the resulting permeability coefficient $D_h f_D(w_c)$ does not represent the flow of water between the two surfaces of a crack but it describes the overall moisture flow through cracked concrete with smeared cracks in which the diffusion properties are completely different respect to the uncracked concrete. Similarly the diffusivity coefficient in Ref. [63] has been modified to include the cracking effect with a good fitting of moisture transport phenomena. For the sake of simplicity, the effect of self-healing on the permeability is neglected in the proposed formulation, but nevertheless, this effect should be introduced into the model but this will be matter of future work.

3. Experimental investigation

The experimental campaign taken here as a reference for the numerical modelling has been described in detail in Ref. [21]. A Normal Strength Concrete, with a target average compressive strength of 30 N/mm^2 (on cubes) and a water-cement ratio equal to 0.55 was taken as a reference, also addressing the influence of a crystalline admixture, employed as self healing promoter at a dosage equal to 1% by weight of cement. The employed crystalline admixtures consists of a mix of proprietary active and highly hydrophilic chemicals in a carrier of cement and sand. The active chemicals react with water and cement and with cement hydration products, mainly calcium hydroxide, to produce calcium silicate hydrates which, be-side refining the concrete matrix pore structure have also exhibited crack healing functionalities. Details about the chemical composi-tion of the employed admixture can be found in Ref. [21]. The self-healing evaluation methodology employed unnotched prismatic beam specimens (500 mm $\times$ 100 mm $\times$ 50 mm) pre-cracked in three-point bending up to two different crack opening levels, respectively equal to 0.15 and 0.30 mm, and then either stored in water or left exposed to open air up to 12 months. Three-point bending tests were repeated up to failure after scheduled conditioning periods. Self-healing was thus evaluated by comparing the peak-load bearing capacity exhibited by the specimens after conditioning to the residual one the same specimens featured upon pre-cracking when unloaded at the prescribed crack opening. The TPB experimental set-up is presented in Fig. 4a together with the spec-imen conditioning, either by immersing them in water (4b) or exposing them to open air (4c). For the characteristics of the employed crystalline admixture as well as for a detailed analysis of the results, including SEM observation and characterization of the healing products the reader is referred to [21].

4. Numerical simulations

4.1. Numerical implementation

The proposed model is numerically implemented in a finite element framework which is composed of two main parts: (1) a finite element solver for the integration of the hygral-thermal-chemical problem including the calculation of the internal variables and using the crack opening values if greater than w_{c0} from mechanical problem; and (2) a finite element solver for the solution of the mechanical problem given the solution of the hygral-thermal-chemical problem. It must be observed that, despite the original formulation [17], the two problems are now coupled and consequently the two numerical solutions must be carried out in

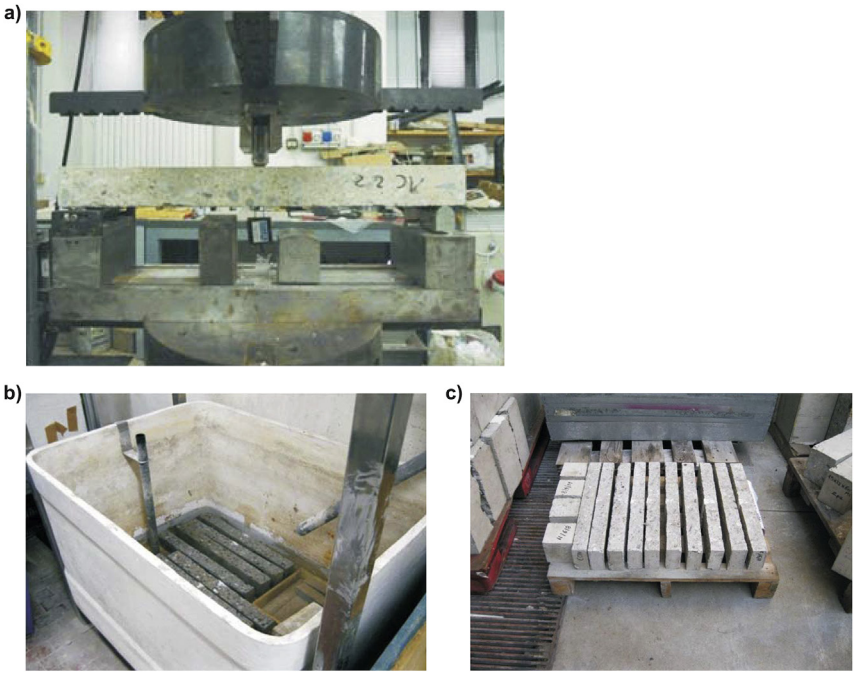

Fig. 4. TPB test set-up (a); (b) specimens immersed in water after cracking; (c) specimens exposed in external air after cracking.

parallel staggering the solution of the hygral-thermal-chemical according the loading history. As consequence, the convergence is obtained independently within the hygral-thermal-chemical part and the mechanical part taking as constant input the information that exchange each other. The numerical integration of the hygral-thermal-chemical problem was presented thoroughly in Ref. [17] where the interested reader can find all the details. The numeri-cal implementation of the finite element solution of the nonlinear mechanical problem was discussed rigorously in Refs. [52] and [15] to which the reader is referred for details.

4.2. Model calibration

The procedure for the calibration of the parameter of the hygro-thermo-chemical (HTC) model was discussed minutely in Ref. [17]. Because the experimental data necessary to calibrate the HTC parameters are not available with reference to the concrete herein investigated see Sect. 3 and [21], an educated guess of the parameter values is therefore necessary. In the presented study the following HTC parameters were used based on the previous experience on model calibration: ρ =2400 kg/m^3; c_t =1100 J/kg°C; λ_t =5.4 W/m°C; $\tilde{Q}_c^{\infty}$ =500 kJ/kg; $\tilde{Q}_s^{\infty}$ =780 kJ/kg; E_{ac}/R =5000 K; E_{as}/R =9700 K; E_{ad}/R =2700 K; SF^{eff} =0.9; κ_c =0.253; g_1 =1.3; k_{vg}^c =0.2; k_{vg}^s =0.3; A_{c1} =3·10^7 h^{-1}; A_{c2} =1·10^{-4}; η_c =5.5; A_{s1} = 20·10^{11} h^{-1}; A_{s2} =1·10^{-6}; η_s =9.5; D_0 =3.6·10^{-10} [kg/mm h]; D_1 =2.5·10^{-7} [kg/mm h]; n = 4.5.

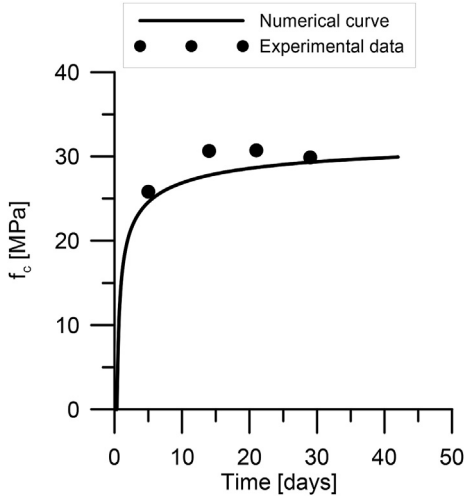

Fig. 5. Evolution of the compressive strength.

The new parameters of the self-healing recovery degree (see Eqs. (8) and (10)) have been determined from the best fitting of the load-crack opening displacement curves presented in the next section. From the best fitting the following values were obtained: $\tilde{A}_{sh1}$ = 3·10^3 kg/m^{3}h, $\tilde{A}_{sh2}$ = 3.25·10^4 kg/m^{3}h, a_w = 3, b_w = 4, and E_{sh}/R = 5000 K.

The response of the mechanical model (Solidification-Micro-prestress-Microplane model) is also governed by some material parameters that must be calibrated from the best fitting of relevant experimental data. The calibration and validation of the SMM model parameters have been already presented in a previous publications [15,64]. Briefly this procedure is hereafter described. From the best fitting of experimental data on basic creep relevant to at least two concrete ages the basic creep parameters, q_1, q_2, q_4, and n_α, can be identified. For the calibration of parameters κ_0, and κ_1 creep data at variable humidity and temperature, such as drying creep and/or transitional thermal creep, are needed. The coefficients k_t and k_{sh} can be identified from experimental data on thermal expansion/contraction and shrinkage, respectively. The parameters of the aging microplane model, which control the aging strength (uniaxial and multiaxial) and the fracture energy, $k1^{\infty}$, $k2^{\infty}$, $k3^{\infty}$, $k4^{\infty}$, $k5^{\infty}$, $k6^{\infty}$, $k7^{\infty}$, k_6^0, λ_0, α_0, A_λ and n_λ, n_7, can be obtained through fitting experimental data relevant to unconfined compressive strength, triaxial tests, and fracture tests at different ages. Once the model has been calibrated, the model validation can be performed by simulating experimental data, concerning the same concrete of the calibration, that has not been used in the calibration procedure and therefore parameters can not be changed. Since in the experimental campaign considered in this work (see Sect. 3) almost all those mechanical properties have not been investigated, the SMM model parameters used in the numerical simulations have been assumed from similar concrete as reported in the following: q_1 = 1.15 ·10^{-5}MPa^{-1}, q_2 = 2.6·10^{-5} MPa^{-1}, n_α = 1.2, q_4 = 1 ·10^{-6}MPa^{-1}, κ_0 = 1·10^{-2} MPa^{-1} day^{-1}, κ_1 = 5 MPa/K, $k1^{\infty}$ = 212·10^{-6} $k2^{\infty}$ = 500, $k3^{\infty}$ = 10, $k4^{\infty}$ = 150, $k5^{\infty}$ = 0.6, k_6^0 = 1.74, $k6^{\infty}$ = 0.87, λ_0 = 0.5, $k7^{\infty}$ = 200, n_7 = 1.0, k_{sh} = 2.5·10^{-3}, k_t = 1·10^{-5}, E = 44000 MPa.

Differently, the parameters of the aging degree have been obtained through the best fitting of the experimentally measured evolution of the compressive strength, as shown in Fig. 5, for the concrete considered in this study. The identified values of those parameters (Eq. (20)) are α_0 = 0.24, A_λ = 3.4, and n_λ = 0.3.

In order to remove spurious mesh sensitivity and to prevent the localization of damage into an area of zero volume, the continuum theory must be enhanced by some additional requirements called

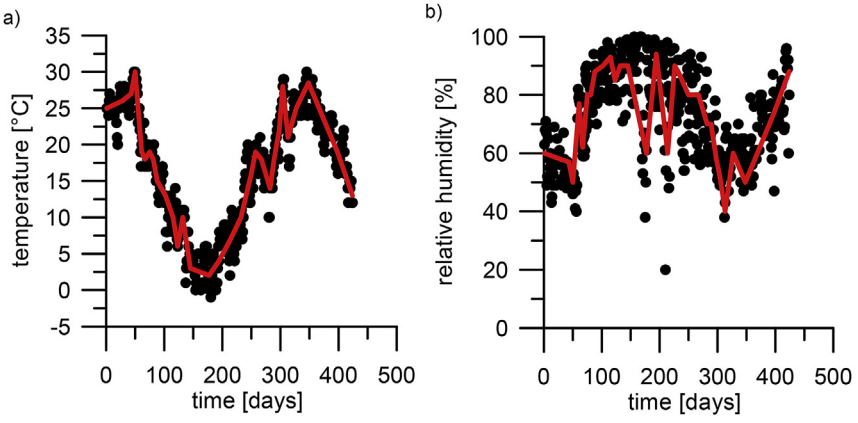

Fig. 6. Evolution of temperature (a) and relative humidity (b) in air and the corresponding interpolation lines utilized as input for the hygro-thermo-chemical model.

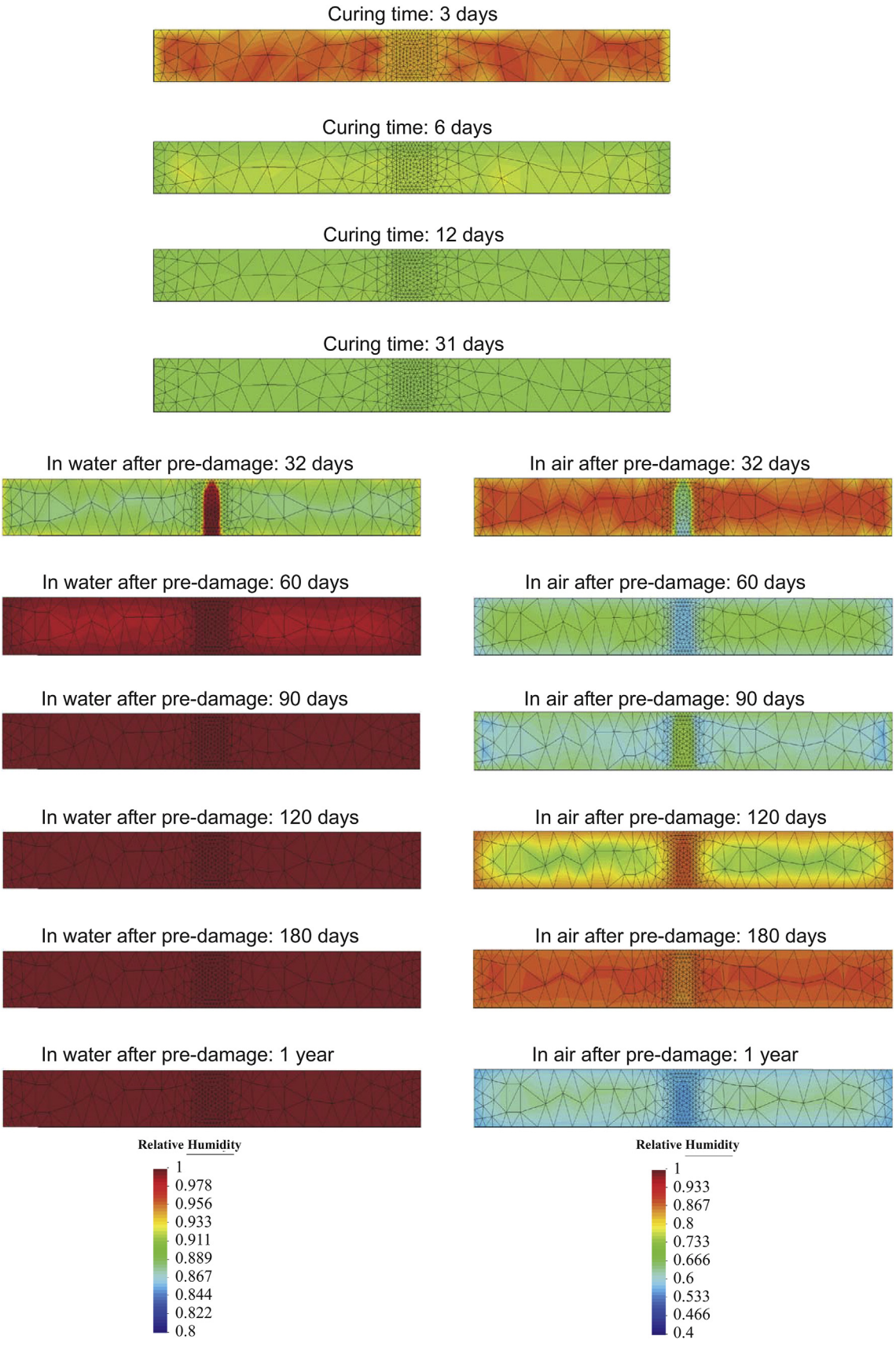

Fig. 7. Relative humidity distribution at different ages in the longitudinal mid-plane of the specimen during the curing period (first 31 days) and during the treatment in water on the left and in the air on the right up to 1 year after the cracking.

'localization limiters' [55]. In this case, the simplest localization limiter, the crack band model [65], is adopted. In the crack band model, which is the model most widely used in practical applications, the post-peak slope of the stress-strain diagram is adjusted as a function of the element size. In the modified microplane model M4 this is achieved by adjusting the free parameter k_5^{∞}

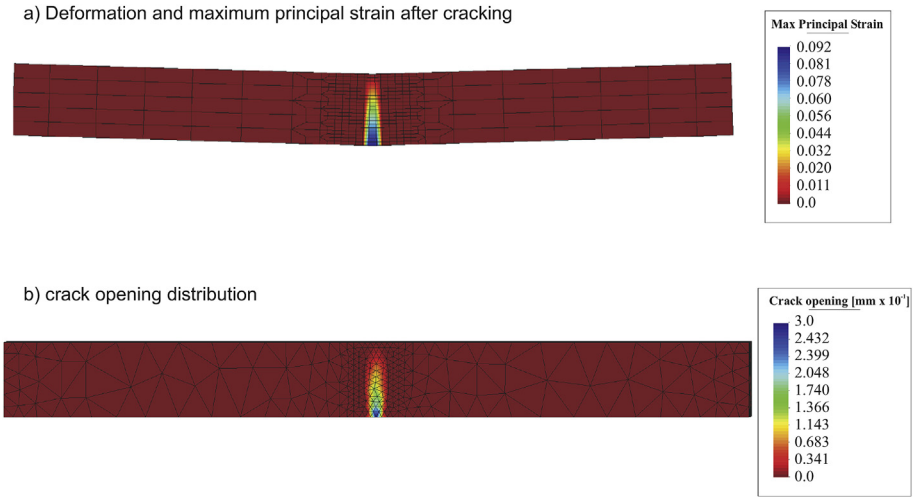

Fig. 8. Damage distribution after the initial cracking in the two meshes of the (a) mechanical model and of the (b) hygro-thermo-chemical model.

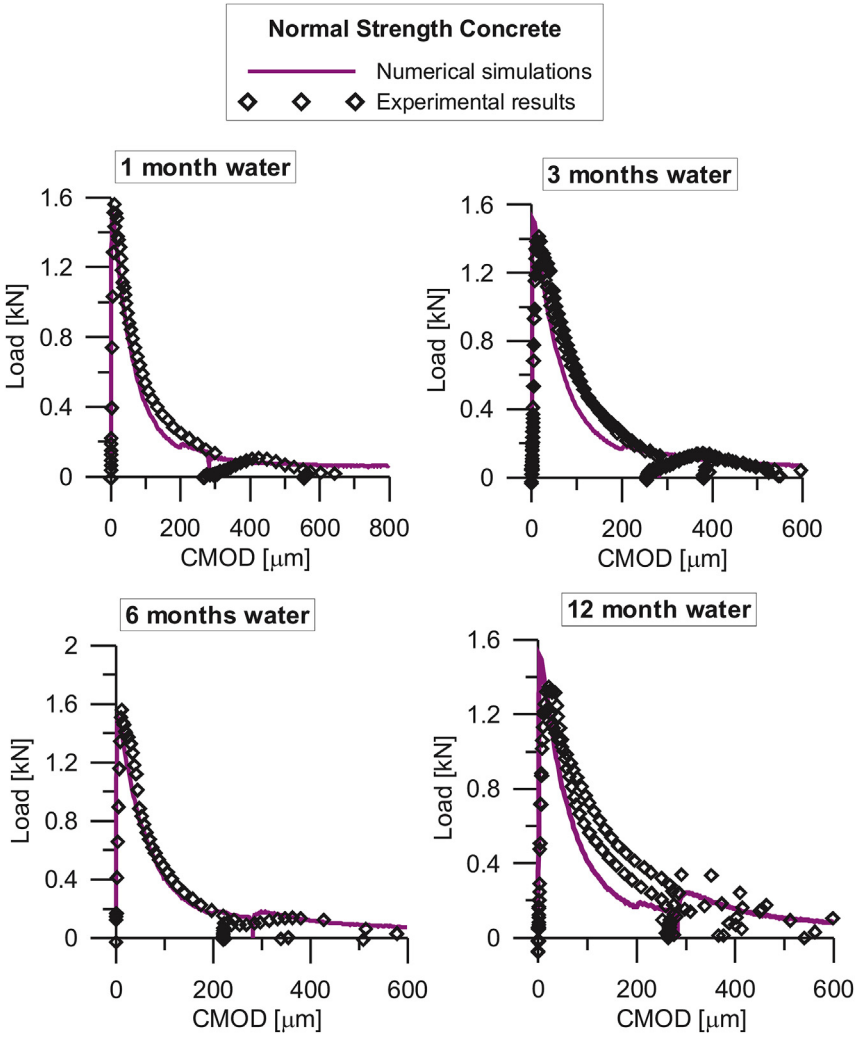

Fig. 9. Load-COD curve obtained with TPB tests from the same specimen before and after the self-healing action in water for the concrete mix with no additive.

according to the crack band width l_c, which, for solid eight node (brick) elements, is assumed to be equal to the average element size $l_c = V^{1/3}$, where V is the volume of the finite element.

However, this simple remedy from spurious mesh sensitivity presents some limitations and shortcomings. The band width based on the cubic root of the element volume does not take into account that the actual effective width of the localized crack band, which forms in a finite element analysis, is affected by the element type, element shape, direction of the crack band with respect to the mesh lines and, for higher-order elements, even by the integration scheme. In the numerical analysis presented in the manuscripts, all these effects are limited since the solid eight node (brick) elements with full integration are adopted, the mesh is aligned with the direction of the crack band, all the elements in the crack band have the same dimensions, no lateral stress in the band, and the fracture energy in the crack band is also checked. For more general formulation of the crack band approach an interested reader can refer to [66].

4.3. Numerical simulations of experimental data

The experimental tests described above in Sect. 3 have been hereafter numerically simulated. The evolution of the temperature, relative humidity, degree of hydration, and self-healing recovery degree are obtained from the solution of the hygro-thermo-chemical problem imposing the appropriate environmental conditions before and after the cracking, as described in the previous section. The specimens immersed in water present constant external environmental conditions (temperature of 20°C and relative humidity of 100%). On the contrary, the specimens exposed to open air had variable external environmental conditions as reported in Fig. 6. In Fig. 7 the simulated evolution of the relative humidity for the specimens kept in water and in air after the cracking is shown. It can be observed how after 2 months in water the specimens reach the saturation and, differently, the specimens left outside the laboratory present an internal relative humidity that follows the trends of the ambient one (plotted in Fig. 6b). The numerical analyses start with the mechanical simulations of the three-point-bending tests that stop at a crack opening of 0.28 mm. After that the crack openings are transferred to the hygro-thermo-chemical model as shown in Fig. 8 and the chemo-diffusion analyses are performed. Finally, using those results the mechanical simulations of the three-point-bending tests are performed again up to the complete failure. The comparison between the experi-mental and the numerical results in terms of the load vs. COD response is reported in Figs. 9 and 10 for the concrete mixture without and with the additive, respectively, after a water curing for different time durations. A recovery of the load bearing capacity,

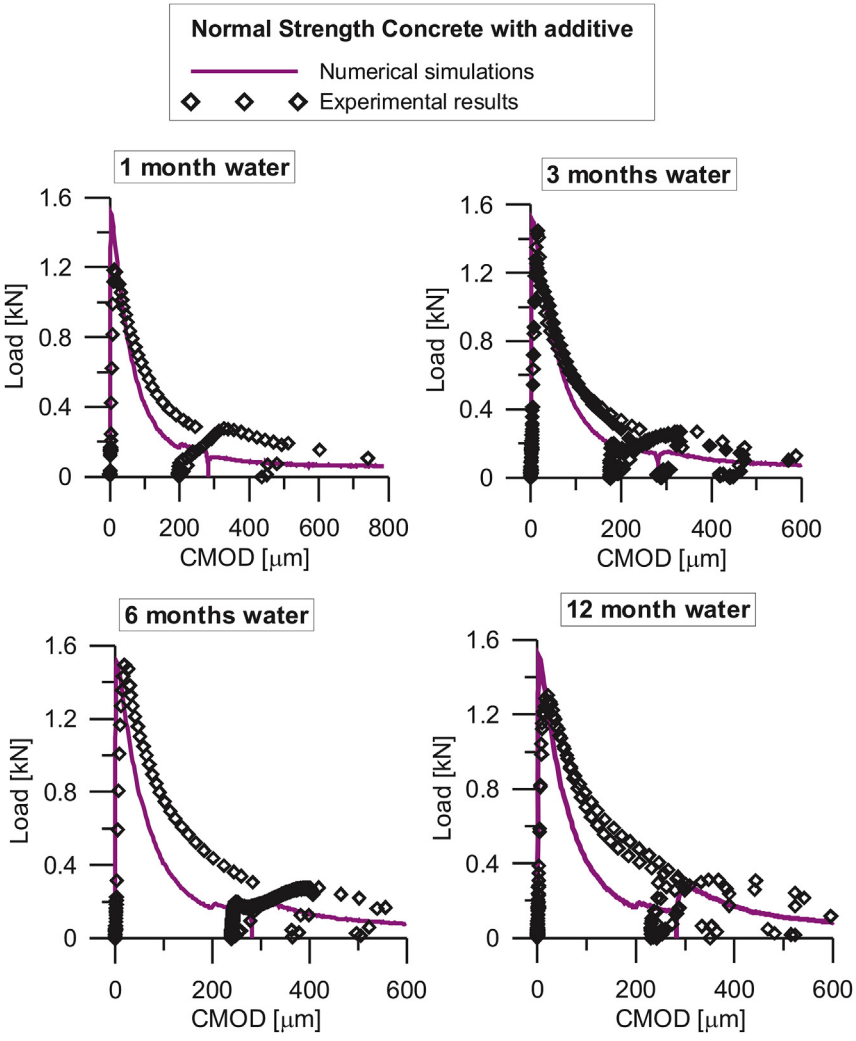

Fig. 10. Load-COD curve obtained with TPB tests from the same specimen before and after the self-healing action in water for the concrete mix with the additive.

with respect to the unloading value at which pre-cracking was performed in the first stage, is evident. It is also clear how the proposed numerical model is capable of simulating the increase of recovering with the increase of curing time in water and also the effect of the additive that enhances the healing process. In Figs. 11 and 12 the experimental and the numerical the load vs. COD curves are plotted for the concrete mixture without and with the additive, respectively, after open air curing for different time durations. Also in this case a recovery of the load bearing capacity is observed but less evident. Again the proposed numerical model is able to reproduce the strength recovering also in this case for different curing time in open air and with and without the presence of the additive in the concrete mixture. All the numerical simulations have been performed using the same set of material parameters that are reported in the previous section.

5. Concluding remarks and further work

In this paper a numerical modelling framework has been proposed to simulate and/or predict self-healing in cement based materials and its outcomes on the recovery, if any, of their mechanical performance. The SMM model has been modified to incorporate the effects of self-healing and three main new features has been introduced: (1) a new internal variable, the self-healing recovery degree, in order to describe the overall self-healing process; (2) the permeability has been made function of the damage and crack opening; (3) the microplane model has been modified in order to consider the recovery of the mechanical properties induced by the healing activity. The model herein proposed was calibrated and validated with reference to a wide experimental campaign, which has investigated the self healing capacity of a normal strength concrete, either containing or not in its mix design a crystalline admixture as a self healing catalyst. The self-healing capacity has been evaluated through the recovery of the post-cracking residual load bearing capacity of specimens cracked and cured for scheduled times in different environments.

The numerical simulations have shown that the proposed model properly describes both the autogenic healing and the autonomic/engineered healing of a cementitious composite in terms of the recovery of load bearing capacity. Nonetheless, some additional features should be introduced in the present formulation, such as the effect of self-healing on the permeability, the presence of through crack stresses (only stress-free cracks have been considered), and the effect of calcium leaching or dissolution.

The SMM model is particularly capable of reproducing the creep and relaxation behavior, especially in the non-linear stage and under variation of temperature and relative humidity. The proposed modifications for self-healing phenomena introduce a

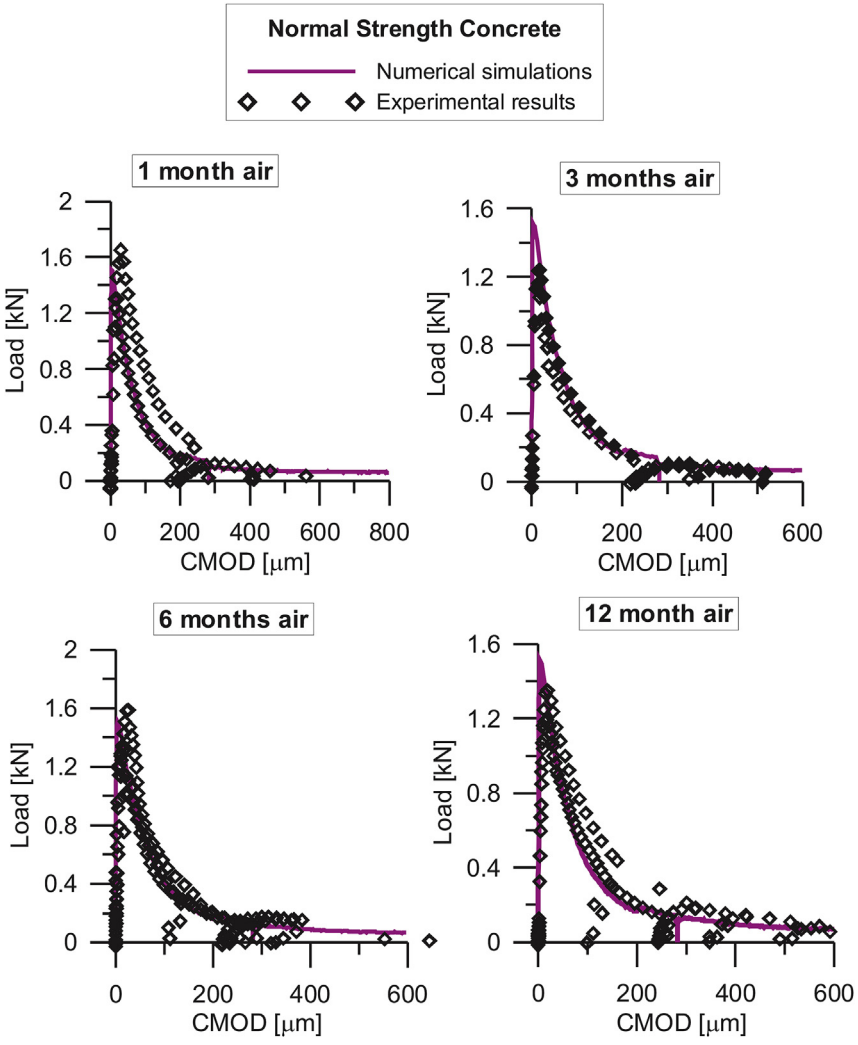

Fig. 11. Load-COD curve obtained with TPB tests from the same specimen before and after the self-healing action in air for the concrete mix with no additive.

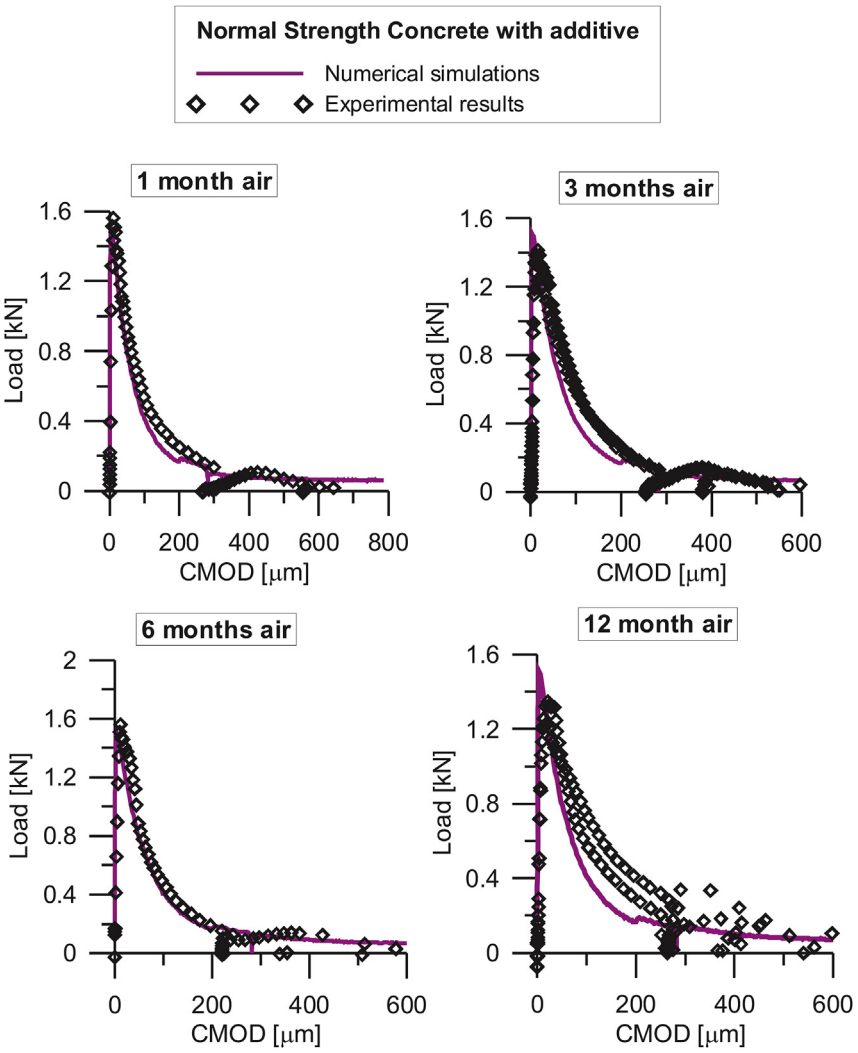

Fig. 12. Load-COD curve obtained with TPB tests from the same specimen before and after the self-healing action in air for the concrete mix with the additive.

change in the evolution of the microcrack growth in which, under sustained mechanical loads, a regain of strength withstand the crack propagation. However, this effect is not studied in this research and it will be undoubtedly subject of future work, especially because this condition represents the true condition for real concrete structures under service loading.

The proposed model represents a first but much needed step toward incorporating self healing concepts and outcomes into design approaches for structures made of and/or retrofitted with cement based materials that possess self-healing functionalities.

Acknowledgments

The authors acknowledge the financial contribution of Politecnico di Milano, Giovani Ricercatori 2011 grant, Self Healing Capacity of Cementitious Composites. The experimental campaign assumed herein as reference has been financially supported by Penetron Italia, whose contribution is gratefully acknowledged.

Appendix A. Moisture Permeability and Evaporable Water

Based on the formulation in Ref. [16], the moisture permeability is formulated as a nonlinear function of the relative humidity h and the temperature T such as

$$D_h(h,T) = \exp\left(\frac{E_{ad}/R}{T_0 - T}\right) D_1 \left[1 + \left(\frac{D_1}{D_0} - 1\right)(1-h)^n\right]^{-1} \tag{22}$$

where $T_0 = 296$ °K, $E_{ad}/R \approx 2700$ K [67].

The evaporable water content, which defines the so-called sorption/desorption isotherm, can be expressed as a function of relative humidity, degree of hydration, and degree of silica fume reaction [68]:

$$w_e(h,\alpha_c,\alpha_s) = G_1(\alpha_c,\alpha_s)\left[1 - \frac{1}{e^{10(g_1\alpha_c^\infty - \alpha_c)h}}\right] + K_1(\alpha_c,\alpha_s) \times \left[e^{10(g_1\alpha_c^\infty - \alpha_c)h} - 1\right] \tag{23}$$

$$G_1(\alpha_c,\alpha_s) = k_{vg}^c \alpha_c c + k_{vg}^s \alpha_s s \tag{24}$$

$$K_1(\alpha_c,\alpha_s) = \frac{w_0 - 0.188\alpha_c c + 0.22\alpha_s s - G_1\left[1 - e^{-10(g_1\alpha_c^\infty - \alpha_c)}\right]}{e^{10(g_1\alpha_c^\infty - \alpha_c)} - 1} \tag{25}$$

where g_1; k_{vg}^c; and k_{vg}^s are material parameters.

Appendix B. Microplane Model Constitutive Equations

In this appendix the microplane constitutive equations of the model adopted in this work are reported. In the following formulae the superscripts "+" and "-" indicate upper (positive value) bounds and lower (negative value) bounds for the different micro-stresses, respectively.

Normal Boundaries

$$F_N^+ = \overline{E}k_1k_6c_1\exp\left(-\frac{\langle\varepsilon_N - k_1k_6c_1c_2\rangle}{k_1k_5k_6c_3 + \langle -c_4\sigma_V/\overline{E}_V\rangle}\right) \quad F_N^- = \begin{Bmatrix} 0 & \text{for } \varepsilon_N > 0 \\ -\infty & \text{for } \varepsilon_N < 0 \end{Bmatrix} \tag{26}$$

where $\langle x\rangle = \max(x,0)$, $\overline{E}_V = \overline{E}/(1-2\nu)$; $c_1 = 0.5$; $c_2 = 0.45$; $c_3 = 3.75$; and $c_4 = 2.5$.

Deviatoric Boundaries

$$F_D^+ = \overline{E}k_1c_5\left[1 + \left\langle\frac{\varepsilon_D - k_1c_5c_6}{k_1k_5k_7c_{20}}\right\rangle^2\right]^{-1} \quad F_D^- = -\overline{E}k_1c_8\left[1 + \left\langle\frac{-\varepsilon_D - k_1c_8c_9}{k_1k_5k_7}\right\rangle^2\right]^{-1} \tag{27}$$

where $\varepsilon_D = \varepsilon_N - \varepsilon_V$ is the deviatoric component of the normal strain; $\varepsilon_V = \varepsilon_{ii}/3$ is the volumetric strain; $c_5 = 2.3$; $c_6 = 2.2$; $c_8 = 4.9$; $c_9 = 0.75$; and $c_{20} = 0.05$.

Volumetric Boundary

$$F_V^- = -\overline{E}k_1k_3\exp\left[-\varepsilon_V/(k_1k_4)\right] \tag{28}$$

Shear Boundary

$$F_T = \frac{\overline{E}_Tk_1k_2c_{10}\langle -\sigma_N + \sigma_N^0\rangle}{\overline{E}_Tk_1k_2 + c_{10}\langle -\sigma_N + \sigma_N^0\rangle}; \sigma_N^0 = \overline{\sigma}_N^0\exp\left(-\frac{\langle\varepsilon_I - \varepsilon_I^0\rangle}{c_{12}k_5}\right) \tag{29}$$

where $\overline{E}_T = \overline{E}/(1+\nu)$; $\overline{\sigma}_N^0 = \overline{E}_Tk_1k_6c_{11}$; $\varepsilon_I =$ maximum principal strain; $\varepsilon_I^0 = k_1k_6c_{21}$; $c_{10} = 0.75$; $c_{11} = 0.95$; $c_{12} = 0.02$; $c_{21} = 0.51$.

Transition function

$$\varphi = 1 - \exp\left(-c_{15}\sin\left[\frac{\pi}{2}\min\left(\left\langle\sigma_I + \sigma_{I0}\right\rangle\sigma_{I0}^{-1}; 1\right)\right]\left\langle\varepsilon_V - \varepsilon_{V0}\right\rangle\varepsilon_{V0}^{-1}\right) \tag{30}$$

if $\varepsilon_{III} > -\varepsilon_{III0}$; and $\varphi = 0$ if $\varepsilon_{III} \le -\varepsilon_{III0}$; where $\sigma_I =$ maximum principal stress; $\varepsilon_{III} =$ minimum principal strain; $\sigma_{I0} = \overline{E}k_1k_6c_{13}$; $\varepsilon_{V0} = k_1k_6c_{14}$; $\varepsilon_{III0} = k_1k_6c_{19}$; $c_{13} = 0.05$; $c_{14} = c_{15} = 0.5$; and $c_{19} = 6.06$.

The transition function is utilized to compute the normal stress as $\sigma_N = \varphi\sigma_N^{\text{no split}} + (1-\varphi)\sigma_N^{\text{split}}$ where $\sigma_N^{\text{no split}}$ and σ_N^{split} are the normal microplane stresses obtained from the no-split formulation and the formulation with the volumetric-deviatoric split, respectively. For additional details see Ref. [50].

The parameter k_1 expands or contracts in the radial direction all the stress-strain boundaries. The parameter k_2 governs the behavior under high shear deformation or high level of normal compression typically when macroscopic compressive confinement is applied. The parameters k_3 and k_4 control the volumetric stress boundary in compression governing the behavior under high compressive volumetric stresses. Because the first four parameters characterize physically the behavior of C-S-H and its internal structure, it is reasonable to assume the following relations:

$$k_1/k_1^\infty = k_2/k_2^\infty = k_3/k_3^\infty = k_4/k_4^\infty = \lambda \tag{31}$$

where k_1^∞, k_2^∞, k_3^∞, are k_4^∞ are the asymptotic values, i.e. reached at complete hydration, of the parameters. The parameter k_5, which is assumed to be approximately age independent, $k_5 \approx k_5^\infty =$ constant, governs the post peak slopes of normal and deviatoric boundaries as well as the rate of shear behavior degradation due to tensile fracturing. Macroscopically, this parameter changes the softening branch slope of both tension and compression stress-strain curves.

The parameter k_6 produces a vertical change in the normal stress boundary in Eq. (26) and in the frictional cohesion in Eq. (29). It affects also the so called "transition function" in Eq. (30). In the macroscopic behavior, increasing k_6 an increase of the tensile strength is produced without significantly changing the compressing strength. Thus, the parameter k_6 can be adopted to control the ratio between tensile strength and compression strength during the aging, this can be done by setting

$$k_6 = \begin{cases} k_6^0 - \left(k_6^0 - k_6^\infty\right)\lambda/\lambda_0 & \text{for } 0 \le \lambda \le \lambda_0 \\ k_6^\infty & \text{for } \lambda_0 \le \lambda \le 1 \end{cases} \tag{32}$$

where k_6^0, and k_6^∞ are initial and asymptotic values, respectively, of the k_6 parameter.

The parameter k_7 controls the softening behavior of the deviatoric boundaries and, when the other parameters are kept constant, it modifies mainly the post-peak softening of macroscopic uniaxial compression: the greater k_7 the less steeper the macroscopic post-peak slope in compression. This parameter k_7 can be then adopted to simulate the reduction of ductility due to aging by assuming $k_7/k_7^\infty = \lambda^{-n_7}$.

References

[1] TC RILEM 221-SHC, Self-healing Phenomena in Cement-based Materials State-of-the-art Report of RILEM Technical Committee 221-SHC: Self-healing Phenomena in Cement-based Materials, Volume RILEM State-of-the-art Reports, Springer, 2013.

[2] H. Mihashi, T. Nishiwaki, Development of engineered self-healing and self-repairing concrete-state-of-the-art report, J. Adv. Concr. Technol. 10 (5) (2012) 170–184.

[3] K. van Tittelboom, N. de Belie, Self-healing in cementitious materials. a review, Materials 6 (2013) 2182–2287.

[4] E. Cuenca, L. Ferrara, Self-healing capacity of fiber reinforced cementitious composites. state of the art and perspectives, in press on KSCE, J. Civ. Eng. 21 (7) (2017) 2777–2789.

[5] M. Wu, B. Johannesson, M. Geiker, A review: self-healing in cementitious materials and engineered cementitious composite as a self-healing material, Constr. Build. Mater. 28 (2012) 571–583.

[6] Z. Lv, D. Chen, Overview of recent work on self-healing in cementitious materials, Mater. Construcciòn 64 (2014) 12.

[7] D. Snoeck, N.D. Belie, From straw in bricks to modern use of microfibers in cementitious composites for improved autogenous healing. a review, Constr. Build. Mater. 95 (2015) 774–787.

[8] G. Yildirim, O.K. Keskin, S.B. Keskin, S. Sahmaran, M. Lachemi, A review of intrinsic self-healing capability of engineered cementitious composites: recovery of transport and mechanical properties, Constr. Build. Mater. 101 (2015) 10–21.

[9] N. Muhammad, A. Shafagha, A. Keyvanfar, M.A. Majid, S. Ghoshal, S.M. Yasouj, A.A. Ganiyu, M.S. Kouchaksaraei, H. Kamyab, M.M. Taheri, M.R. Shirdar, R.M. Caffer, Tests and methods of evaluating the self-healing efficiency of concrete: a review, Constr. Build. Mater. 112 (2016) 1123–1132.

[10] B. Hilloulin, F. Grondin, M. Matallah, A. Loukili, Modelling of autogenous healing in ultra high performance concrete, Cem. Concr. Res. 6162 (2014) 64–70.

[11] B. Hilloulin, D. Hilloulin, F. Grondin, A. Loukili, N.D. Belie, Mechanical regains due to self-healing in cementitious materials: experimental measurements and micro-mechanical model, Cem. Concr. Res. 80 (2016) 21–32.

[12] A. Aliko-Benítez, M. Doblar, J. Sanz-Herrera, Chemical-diffusive modeling of the self-healing behavior in concrete, Int. J. Solids Struct. 69–70 (2015) 392–402.

[13] R. Davies, A. Jefferson, Micromechanical modelling of self-healing cementitious materials, Int. J. Solids Struct. 113–114 (2017) 180–191.

[14] A. Caggiano, V. Krelani, L. Ferrara, G. Etse, A zero-thickness interface formulation for modeling the self-healing effects on the recovery of mechanical properties of concrete, Comput. Struct. 186 (2017) 22–34.

[15] G. Di Luzio, G. Cusatis, Solidification-Microprestress-Microplane (SMM) theory for concrete at early age: theory, validation and application, Int. J. Solids Struct. 50 (2013) 957–975.

[16] G. Di Luzio, G. Cusatis, Hygro-thermo-chemical modeling of high performance concrete. I: Theory, Cem. Concr. Compos. 31 (2009a) 301–308.

[17] G. Di Luzio, G. Cusatis, Hygro-thermo-chemical modeling of high performance concrete. II: numerical implementation, calibration, and validation, Cem. Concr. Compos. 31 (2009b) 309–324.

[18] G. Di Luzio, L. Ferrara, V. Krelani, A numerical model for the self-healing capacity of cementitious composites, in: N. Bicanic, H. Mang, G. Meschke, R. e de Borst (Eds.), Proceedings of Computational Modelling of Concrete Structures - EURO-c 2014, CRC Press/Balkema, Leiden, St. Anton Am Arlberg; Austria, March 24-27, 2014, 2014, pp. 741–747.

[19] G. Di Luzio, L. Ferrara, V. Krelani, Numerical simulation of self-healing in cementitious composites, in: H. Furuta, D.M. Frangopol, M. e Akiyama (Eds.), Proceedings of Fourth International Symposium on Life-cycle Civil Engineering (IALCCE2014), Tokyo, Japan, November 16-19, 2014, pp. 1–7.

[20] G. Di Luzio, V. Krelani, L. Ferrara, Numerical simulation of self-healing process and its application, in: M. Colombo, M. di Prisco (Eds.), Proceedings of the 8Th International Conference on Concrete under Severe Conditions-environment & Loading (CONSEC2016), Lecco, Italy, September 12-14, 2016, pp. 38–45.

[21] L. Ferrara, V. Krelani, M. Carsana, A "fracture testing" based approach to assess crack healing of concrete with and without crystalline admixtures, Constr. Build. Mater. 68 (2014) 535–551.

[22] F.J. Ulm, O. Coussy, Modeling of thermochemomechanical couplings of concrete at early ages, J. Engrg. Mech. ASCE 121 (1995) 785–794.

[23] M. Cervera, J. Oliver, T. Prato, Thermo-chemo-mechanical model for concrete. I: hydration and aging, J. Eng. Mech. ASCE 125 (1999) 1018–1027.

[24] D. Gawin, F. Pesavento, B.A. Schrefler, Hygro-thermo-chemo-mechanical modelling of concrete at early ages and beyond. part i: hydration and hygro-thermal phenomena, Int. J. Numer. Methods Eng. 67 (2006) 299–331.

[25] S. Pantazopoulo, R. Mills, Microstructural aspects of the mechanical response of plain concrete, ACI Matererials J. 92 (6) (1995) 605–616.

[26] C. Edvardsen, Water Permeability and Self-healing of Through-crack in Concrete. (In German), DAfStb Bull. 455, Berlin, 1996.

[27] L. Ferrara, V. Krelani, F. Moretti, Autogenous healing on the recovery of mechanical performance of high performance fibre reinforced cementitious composites (HPFRCCs): Part 2 – correlation between healing of mechanical performance and crack sealing, Cem. Concr. Compos. 73 (2016) 299–315.

[28] L. Ferrara, V. Krelani, F. Moretti, M.R. Flores, P.S. Ros, Effects of autogenous healing on the recovery of mechanical performance of high performance fibre reinforced cementitious composites (hpfrccs): Part 1, Cem. Concr. Compos. 83 (2017) 76–100.

[29] L. Ferrara, V. Krelani, F. Moretti, On the use of crystalline admixtures in cement based construction materials: from porosity reducers to promoters of self healing, Smart Mater. Struct. 25 (2016) 084002.

[30] K. Lauer, F. Slate, Autogenous healing of cement paste, ACI J. 52 (1956) 1083–1097.

[31] P.W. Atkins, Physical Chemistry, fifth ed., Oxford University Press, Oxford, U.K, 1994.

[32] C. Edvardsen, Water permeability and autogenous healing of cracks in concrete, ACI Matererials J. 96 (1999) 448–455.

[33] H. Reinhardt, M. Jooss, Permeability and self-healing of cracked concrete as a function of temperature and crack width, Cem. Concr. Res. 33 (2003) 981985.

[34] K. Wang, D. Jansen, S. Shah, A. Karr, Permeability study of cracked concrete, Cem. Concr. Res. 27 (1997) 381–393.

[35] S. Granger, A. Loukili, G. Pijaudier-Cabot, G. Chanvillard, Experimental characterization of the self-healing of cracks in an ultra high performance cementitious material: mechanical tests and acoustic emission analysis, Cem. Concr. Res. 37 (2007) 519–527.

[36] D. Hannant, J. Keer, Autogenous healing of thin cement based sheets, Cem. Concr. Res. 13 (1983) 357–365.

[37] R. Dhir, C. Sangha, J. Munday, Strength and deformation properties of autogenously healed mortars, ACI J. 3 (1973) 231–236.

[38] S. Jacobsen, E. Sellevold, Self healing of high strength concrete after deterioration by freeze/thaw, Cem. Concr. Res. 26 (1995) 55–62.

[39] M.Şahmaran, S. Keskin, G. Ozerkan, I. Yaman, Self-healing of mechanically-loaded self consolidating concretes with high volumes of fly ash, Cem. Concr. Compos. 30 (2008) 872–879.

[40] C. Clear, The Effects of Autogenous Healing upon the Leakage of Water through Cracks in Concrete, Cement and Concrete Association, Slough, U.K, 1985, p. 28.

[41] N. Ter Heide, Crack Healing in Hydrating Concrete., Master Thesis, Delft University of Technology, Delft, The Netherlands, 2005.

[42] L. Ferrara, I. Albertini, R. Gettu, V. Krelani, S. Moscato, F. Pirritano, M. Roig Flores, P. Serna, S. Theeda, Self healing of cement based materials engineered through crystalline admixtures: results from a multinational university network, in: e. M.A. Chiorino, et al. (Eds.), ACI Special Publication 305. Durability and Sustainability of Concrete Structures – Workshop Proceedings, Bologna, Italy, October 1-3, 2015, 13.1–13.10.

[43] M. Roig-Flores, S. Moscato, P. Serna, L. Ferrara, Self-healing capability of concrete with crystalline admixtures in different environments, Constr. Build. Mater. 86 (2015) 1–11.

[44] M. Roig-Flores, F. Pirritano, P. Serna, L. Ferrara, Effect of crystalline admixtures on the self-healing capability of early-age concrete studied by means of permeability and crack closing tests, Constr. Build. Mater. 114 (2016) 447–457.

[45] Z.P. Bažant, S. Baweja, Creep and shrinkage prediction model for analysis and design of concrete structures-Model B3, Mater. Struct. 28 (1995) 357–365.

[46] Z.P. Bažant, S. Prasannan, Solidification theory for concrete creep. I: formulation, J. Eng. Mech. ASCE 115 (1989) 1691–1703.

[47] Z.P. Bažant, A.B. Hauggaard, S. Baweja, F.J. Ulm, Microprestress-solidification theory for concrete creep. I: aging and drying effects, J. Eng. Mech. ASCE 123 (1997) 1188–1194.

[48] Z.P. Bažant, G. Cusatis, L. Cedolin, Temperature effect on concrete creep modeled by microprestress-solidification theory, J. Eng. Mech. 130 (2004) 691–699.

[49] Z.P. Bažant, F.C. Caner, I. Carol, M.D. Adley, S.A. Akers, Microplane model M4 for concrete. I: formulation with work-conjugate deviatoric stress, J. Eng. Mech. ASCE 126 (9) (2000) 944–953.

[50] G. Di Luzio, A symmetric over-nonlocal microplane model m4 for fracture in concrete, Int. J. Solids Struct. 44 (2007) 4418–4441.

[51] G. Cusatis, A. Beghini, Z. Bažant, Spectral stiffness microplane model for quasi-brittle composite laminates: I. theory, J. Appl. Mech. ASME 75 (2008) 021009–021009–9.

[52] G. Di Luzio, Numerical model for time-dependent fracturing of concrete, J. Eng. Mech. ASCE 135 (2009) 632–640.

[53] G. Di Luzio, G. Muciaccia, L. Biolzi, Size effect in thermally damaged concrete, Int. J. Damage Mech. 19 (2010) 631–656.

[54] G. de Schutter, L. Taerwe, Degree of hydration based description of mechanical properties of early age concrete, Mater. Struct. 29 (1996) 335–344.

[55] G. Di Luzio, Z.P. Bažant, Spectral analysis of localization in nonlocal and over-nonlocal materials with softening plasticity or damage, Int. J. Solids Struct. 42 (2005) 6071–6100.

[56] A. Neville, Properties of Concrete, John Wiley and Sons, New York, 1997.

[57] J.-K. Kim, C.-S. Lee, Moisture diffusion of concrete considering self-desiccation at early age, Cem. Concr. Res. 29 (1999) 1921–1927.

[58] B. Persson, Hydration and strength of high performance concrete, Adv. Cem. Based Mater. 3 (1996) 107–123.

[59] B. Persson, Moisture in concrete subjected to different kinds of curing, Mater. Struct. 30 (1997) 533–544.

[60] T. Ayano, F.H. Wittmann, Drying, moisture distribution, and shrinkage of cement based materials, Mater. Struct. 35 (2002) 134–140.

[61] C. Aldea, M. Ghandehari, S. Shah, A. Karr, Estimation of water flow through cracked concrete under load, ACI Matererials J. 97 (2000) 567–575.

[62] B. Gérard, D. Breysse, A. Ammouche, O. Houdusse, O. Didry, Cracking and permeability of concrete under tension, Mater. Struct. 29 (1996) 141–151.

[63] J. Ožbolt, G. Balabanic, G. Periškic, M. Kušter, Modelling the effect of damage on transport processes in concrete, Constr. Build. Mater. 24 (2010) 1638–1648.

[64] G. Di Luzio, G. Cusatis, Calibration and validation of a numerical model for early age damage analysis, in: J. Carrato, J. Burns (Eds.), Structures Congress -20th Analysis & Computation Specialty Conference - ASCE, Volume 1, Chicago, IL, USA, pp. 437–448.

[65] Z.P. Bažant, B.H. Oh, Crack band theory for fracture of concrete, Matériaux Constr. 16 (1983) 155–177.

[66] J. Oliver, A consistent characteristic length for smeared cracking models, Int. J. Numer. Methods Eng. 28 (1989) 61–74.

[67] Z.P. Bažant, Thermodynamics of interating continua with surfaces and creep analysis of concrete structures, Nucl. Engrg. Des 20 (1972) 477–505.

[68] K. Norling Mjonell, A model on self-desiccation in high-performance concrete, in: Self-desiccation and its Importance in Concrete Technology, Proceedings of the International Research Seminar, Lund, Sweden, 1997, pp. 141–157.